

Decentralized Learning Strategies for Estimation Error Minimization with Graph Neural Networks

Xingran Chen, Navid NaderiAlizadeh, Alejandro Ribeiro, Shirin Saeedi Bidokhti

Abstract—We address the challenge of sampling and remote estimation for autoregressive Markovian processes in a multi-hop wireless network with statistically-identical agents. Agents cache the most recent samples from others and communicate over wireless collision channels governed by an underlying graph topology. Our goal is to minimize time-average estimation error and/or age of information with decentralized scalable sampling and transmission policies, considering both oblivious (where decision-making is independent of the physical processes) and non-oblivious policies (where decision-making depends on physical processes). We prove that in oblivious policies, minimizing estimation error is equivalent to minimizing the age of information. The complexity of the problem, especially the multi-dimensional action spaces and arbitrary network topologies, makes theoretical methods for finding optimal transmission policies intractable. We optimize the policies using a graphical multi-agent reinforcement learning framework, where each agent employs a permutation-equivariant graph neural network architecture. Theoretically, we prove that our proposed framework exhibits desirable transferability properties, allowing transmission policies trained on small- or moderate-size networks to be executed effectively on large-scale topologies. Numerical experiments demonstrate that (i) Our proposed framework outperforms state-of-the-art baselines; (ii) The trained policies are transferable to larger networks, and their performance gains increase with the number of agents; (iii) The training procedure withstands non-stationarity even if we utilize independent learning techniques; and, (iv) Recurrence is pivotal in both independent learning and centralized training and decentralized execution, and improves the resilience to non-stationarity in independent learning.

I. INTRODUCTION

Remote sensing and estimation of physical processes have garnered considerable interest in the realm of wireless networks. Timely estimation of processes and maintaining current knowledge of the system state are critical in numerous applications such as robot swarm control, autonomous vehicle communication, and environmental monitoring [2], [23]. Having fresh and up-to-date information regarding the system state is essential for ensuring effective monitoring and control performance. Additionally, in such applications, it is no longer realistic to assume that information bits are processed and stored at the sources, waiting to be reliably transmitted and replicated at the receiver(s) with a high rate and low latency.

Xingran Chen is with the School of Information and Communication Engineering, University of Electronic Science and Technology of China, Chengdu, China. E-mail: xingranc@ieee.org.

Navid NaderiAlizadeh is with the Department of Biostatistics and Bioinformatics, Duke University, NC 27705. E-mail: navid.naderi@duke.edu.

Alejandro Ribeiro and Shirin Saeedi Bidokhti are with the Department of Electrical and Systems Engineering, University of Pennsylvania, PA, 19104. E-mail: {aribeiro, saeedi}@seas.upenn.edu.

This work was supported by Grants xxx.

This is because information is collected and communicated in real time.

In this paper, we address the issue of *real-time sampling and estimation in multi-hop wireless networks* comprising multiple agents. Each agent observes a physical process, modeled by a Gauss-Markov source [1], [2], and the objective is for all agents to obtain timely estimates of all other sources. This is particularly pertinent in robotic applications, where each agent (robot) requires up-to-date information about all other agents (including their status, location, etc.) for planning and collaboration. Solving this problem involves two steps: (i) *sampling and transmission*, and (ii) *estimation*. Sampling and transmission entail each sensor determining its sampling timestamp, transmission probability, transmission destination, and transmitted packets in each time slot. Estimation involves each sensor reconstructing estimates for the physical processes of all other sensors based on all previously received status updates.

We concentrate on the transmission step and its optimization, as suggested by [2]–[4], emphasizing the optimality of the Kalman-like estimator. Two primary challenges stand out: (i) achieving timely packet transmission in channels with limited capacity, and (ii) facilitating decentralized packet transmission. To capture timeliness, we employ the Age of Information (AoI) metric [5], widely acknowledged in the literature. It is worth noting, as highlighted in [1], [6], that the time-average AoI is intimately linked with the time-average estimation error. Consequently, both metrics play pivotal roles in crafting real-time sampling and transmission policies. Prior research approaches to this problem are mostly built on centralized scheduling policies [7]. However, it is not practical to centrally schedule transmissions, especially when (i) the number of agents is very high, (ii) the network topology is complex, and (iii) the policy space is high-dimensional. Therefore, our objective is to devise efficient *decentralized* policies that minimize both AoI and/or estimation error, while ensuring *scalability*.

This problem has recently been studied for random access collision channels where all the agents communicate with a central fusion [1], [8]–[12]. The authors in [8], [9] have proposed decentralized age-based sampling and transmission policies, with performance guarantees. [10] has developed update strategies requiring only one-bit of information per update that employ a local cancellation strategy. Moreover, the work in [1] has generalized those results by going beyond AoI and has provided (asymptotically) near-optimal policies that minimize the estimation error. The above analytical works heavily build on the topology of the random access channel

(which is a one-hop many-to-one network) and do not extend to more general wireless networks. In [11], [12], the network topologies are considered for decision-making, but both papers investigate centralized policies. It has remained open to obtain near-optimal decentralized mechanisms in ad-hoc networks.

The analysis conducted in the aforementioned papers falls short in our setting, primarily due to the intractability of analytical solutions, especially when confronted with complex and large-scale network topologies. This limitation serves as a compelling motivation for adopting learning-based approaches. In particular, multi-agent reinforcement learning (MARL) algorithms have achieved massive success in many applications that use reinforcement learning (RL) techniques to co-train a set of agents in a multi-agent system [13]. In the real-time sampling and estimation problem, every agent is trained to find its optimal sampling and transmission policies through MARL techniques. However, classical MARL methods, parameterized by multi-layer perceptrons (MLPs), are inappropriate due to the lack of permutation-equivariance and scalability. Consider a classical MARL framework. Note that the input of this framework is the collection of features of nodes in a graph. Since the classical MARL framework is not permutation-equivariant, the output of the framework may change once we permute the ordering of the nodes, even if the environment remains the same. To remedy this issue, we utilize techniques from graph neural networks (GNNs) [14], [15], which are permutation-equivariant by construction, hence leading to a graphical MARL framework.

A. Related Work

1) *Decentralized Age-based Transmission Policies in Multi-hop Networks*: The concept of the Age of Information (AoI), as introduced in [16], serves as a metric for assessing the freshness of information on the receiver side. Early work on AoI considered point-to-point channels [5]. Later, its applicability was extended to single-hop networks featuring multiple sources, with investigations spanning centralized scheduling [17], [18] as well as decentralized transmission policies [8], [19]. In the realm of multi-hop networks, the majority of prior research has focused on centralized transmission policies, exemplified by studies such as [20], [21]. However, there have been some notable efforts toward exploring decentralized transmission policies. For instance, [22] delineated three classes of policies, among which only one falls under the category of simple decentralized policies, specifically, stationary randomized policy; the remaining two are centralized scheduling policies. In scenarios characterized by harsh environments with no existing communication infrastructure [23], such as those encountered by robots forming ad-hoc networks, the necessity for decentralized operation becomes imperative. Addressing this, [23] proposed a task-agnostic, decentralized, low-latency method for data distribution within ad-hoc networks. While [23] treats all packets as identical, it overlooks the information (apart from freshness) included in them.

2) *Timely Estimation Error and AoI*: The relationship between timely estimation error and AoI is pivotal. In remote

estimation applications, the estimation of a physical process relies on received updates (packets). When estimation occurs using a packet with a small AoI, the instantaneous estimation error tends to be small. Conversely, estimation based on a packet with a large AoI typically results in a large instantaneous estimation error, as discussed in [1]. While numerous papers have delved into problems concerning estimation errors, seeking to minimize estimation errors from the vantage point of AoI presents a promising avenue for research.

In point-to-point channels, [3], [24] represent the pioneering work in studying the minimization of estimation error through age. The authors introduced the optimal stopping time to minimize estimation error for Gauss-Markov processes. Various extensions were explored in follow-up studies, such as [4], [25]. The work in [26] unified the AoI minimization problem and the remote estimation error minimization problem. In addition to AoI, two other pertinent metrics investigated in relation to estimation error are effective age [27] and age of incorrect information [28]. In [27], zero-wait policies and sample-at-change policies were analyzed, while [28] proposed an optimal transmission policy based on constrained Markov decision processes.

In the context of random access channels, [10] developed an optimal update strategy requiring only one bit of information per update, whereas [29] provided approximations of estimation error using the age of incorrect information under slotted ALOHA schemes. The model setting in [10] represents an extreme case compared to that in [29]. Our previous work [1] can be viewed as an extension of [10] and [29], wherein we established the equivalence between AoI and estimation error and proposed sub-optimal threshold transmission policies.

3) *Multi-Agent Reinforcement Learning*: Given our focus on minimizing estimation error in multi-hop networks, traditional theoretical methods like those in [1], [10], [29] become impractical due to the complexity introduced by network topologies and multi-hop transmission, which undermines scalability. In this context, MARL algorithms emerge as a promising alternative. These algorithms train a set of agents within a multi-agent system simultaneously to achieve cooperative or competitive goals. Recent years have witnessed the emergence of numerous MARL algorithms integrating deep learning techniques [13], [30]. Broadly speaking, MARL algorithms can be categorized into three classes [13]: (i) Independent learning: Each agent is trained independently by RL algorithms, without considering the multi-agent structure [31]. (ii) Centralized multi-agent policy gradient: Algorithms such as [32] fall into this category, where centralized training and decentralized execution (CTDE) paradigms are utilized. (iii) Value decomposition algorithms: This category includes algorithms like [33], also employing CTDE paradigms. MARL algorithms have demonstrated their effectiveness in solving sequential decision-making problems across various wireless applications [34], including resource management [35], power allocation [36], edge computing [37], fault-tolerant tracking control [38], and edge caching [39]. To date, there is only one weakly related prior study that formulates the problem of age/estimation error minimization using MARL as an event-driven decision process [40]. However, our framework differs

in that decision-making is not event-driven. In our approach, we employ both independent learning and CTDE techniques to address the complexities of the problem.

4) *Graph Neural Networks*: Graph neural networks (GNNs) have become a popular architecture for information processing in graph signal processing [41], thanks to their theoretical properties inherited from graph convolutional filters. These properties include invariance to permutations, stability to deformations, and scalability to large network sizes [14]. Notably, graph processes inherently encapsulate a temporal dimension, and recurrent neural networks (RNNs) serve as a suitable tool for capturing time dependencies within graph processes. The utilization of RNNs becomes particularly significant when the data elements are both Euclidean and time-dependent [42], [43]. Several implementations of graph recurrent architectures can be found in literature [44]–[46]. In [15], Graph Recurrent Neural Networks (GRNNs) were systematically proven to be permutation-equivariant and stable to perturbations in the underlying graph support. Simulations conducted therein demonstrated that GRNNs outperform both GNNs and RNNs. This underscores the importance of considering both spatial and temporal dependencies of a graph process for effective decision-making. Furthermore, the class of GNNs constructed on graph filters exhibits transferability, a property established through the utilization of graphons. Graphons represent the limit of a sequence of dense undirected graphs [47]. In our context, where the information from all agents forms a graph signal in each time slot, employing a GNN or GRNN formulation becomes essential.

B. Contributions

In this paper, we investigate sampling and remote estimation of M independent Gauss-Markov processes over wireless collision channels within *multi-hop wireless networks* (e.g., ad-hoc networks). At each time slot, every agent makes decisions based on its own information regarding (i) *when to sample*, determining whether to transmit a packet; (ii) *who to communicate with*, selecting a neighbor as the receiver of the transmitted packet; and (iii) *what to transmit*, choosing which packet to send to the receiver. Our goal is to minimize the time-average estimation error and/or time-average age of information by proposing decentralized synchronous sampling and transmission policies. We explore two classes of policies: (i) *oblivious policies*, where decision-making is independent of the physical processes, and (ii) *non-oblivious policies*, where decision-making depends on physical processes [1].

Initially, we formulate the age of information and estimation error for all agents within multi-hop networks in a discrete-time setting. Utilizing the derived expressions for the age of information and estimation error, we prove that in oblivious policies, minimizing estimation error is equivalent to minimizing the AoI. Consequently, we unify the problems of error minimization and age minimization and propose a general solution framework.

Within our solution framework, we encounter two significant challenges: (i) a sharp increase in the learning cost with network size, and (ii) the disorder stemming from the

node permutations in graphs. To address these challenges, we propose a scalable graphical MARL framework, which is an extension of the classical actor-critic framework [48], [49]. Here, we augment the actor and critic with graphical network layers, transforming the actor into a GRNN instead of a recurrent neural network (RNN), and the critic into a GNN rather than a neural network. These modifications ensure that our framework is agnostic to the permutations of agent indices, given the fact that GNNs and GRNNs are permutation-equivariant. Moreover, we introduce an action distribution operator that leverages the output node embeddings of the actor GRNN to generate action distributions for all aforementioned decisions. Notably, the parameter counts in both the actor and critic models are independent of the number of agents in the network due to this formulation. Furthermore, we demonstrate that our framework exhibits the transferability property, facilitated by the characteristics of graphons. This implies that policies trained on small or moderate networks can be effectively applied to large-scale networks, significantly reducing the learning cost.

In our implementations, we employ two widely-used reinforcement learning training methods for the critic: (i) independent learning (e.g., IPPO), wherein each agent possesses a distinct critic trained in a decentralized manner, and (ii) CTDE (e.g., MAPPO), where a centralized critic learns a joint state value function. Numerical experiments unveil key insights: (i) the graphical MARL framework surpasses the classical MARL one, with graphical MARL employing CTDE outperforming independent learning by leveraging global network information. (ii) As anticipated, classical MARL with independent learning succumbs to non-stationarity, whereas graphical MARL with independent learning converges, suggesting its potential to mitigate non-stationarity. (iii) Transferability is affirmed by heightened performance gains in large-scale networks, indicating the superiority of the proposed graphical MARL framework. (iv) Recurrence plays a vital role in both independent learning and CTDE and improves the resilience to non-stationarity in independent learning.

II. SYSTEM MODEL

Consider M statistically identical agents communicating over a connected undirected graph. We denote the graph as $\mathcal{G}_M = (\mathcal{V}_M, \mathcal{E}_M)$, where $\mathcal{V}_M = \{1, 2, \dots, M\}$ denotes the set of agents and \mathcal{E}_M denotes the set of edges among agents. The i^{th} agent and the j^{th} agent are directly connected with each other by an edge if and only if $(i, j) \in \mathcal{E}_M$. Denote ∂_i as the set of neighbors of the i^{th} agent, i.e., $\partial_i = \{j | (i, j) \in \mathcal{E}_M\}$. Letting time be slotted, every agent $i \in \mathcal{V}_M$ observes a physical process $\{X_{i,k}\}_{k \geq 0}$,

$$X_{i,k+1} = X_{i,k} + \Lambda_{i,k}, \quad (1)$$

where $\Lambda_{i,k} \sim \mathcal{N}(0, \sigma^2)$ are i.i.d for all i, k [1], [2]. The processes $\{X_{i,k}\}_{k=0}^{\infty}$ are assumed to be mutually independent across i . By convention, $X_{i,0} = 0$ for all $i \in \mathcal{V}_M$.

All agents can communicate with their neighbors, with each agent communicating with at most one neighbor in a given time slot. Specifically, the i^{th} agent can transmit a packet

to the j^{th} agent in a time slot only if $(i, j) \in \mathcal{E}_M$. If there is no edge between the i^{th} and the j^{th} agents, then they can not communicate with each other directly. The communication medium in every hop is modeled by a collision channel: if two or more agents in proximity simultaneously transmit packets in a time slot, then the packets will interfere with each other and cause a communication failure. We assume a delay of one-time unit in delivery for packets. Let $c_{i,k}^j = 1$ represent the event that collisions happen in the edge (i, j) with the direction from the i^{th} agent to the j^{th} agent in time k , otherwise $c_{i,k}^j = 0$. The collision feedback is only available to the senders. It is worth noting that random access protocols can be broadly divided into two classes: synchronous protocols (e.g., slotted ALOHA) and asynchronous protocols (e.g., CSMA). In this paper, we specifically focus on the class of *synchronous* protocols.

Each agent is assumed to have M *virtual queues*¹, and the queue with index $j \in \mathcal{V}_M$, denoted by $Q_{i,j}$, is utilized to cache the packets from the j^{th} agent at the i^{th} agent. We further assume that the buffer size of $Q_{i,j}$ is one and that an incoming packet from the j^{th} agent can either replace undelivered (old) packets or be discarded. This assumption relies on the fact that the underlying processes that are monitored are Markovian. In other words, the old packets become obsolete if the most recently received packet is known. The indicator $q_{i,k}^j = 1$ implies that $Q_{i,j}$ is occupied by a packet in time k ; otherwise $q_{i,k}^j = 0$. In every time slot, the i^{th} agent can sample its source (to which we refer to as a packet in $Q_{i,i}$) or transmit packets in $\{Q_{i,j}\}_{j \neq i}$ to one of its neighbors. Denote $d_{i,k}^{j,\ell} = 1$ as the indicator such that the i^{th} agent transmits a packet from the ℓ^{th} agent (in $Q_{i,\ell}$) to the j^{th} agent successfully at time k , otherwise $d_{i,k}^{j,\ell} = 0$. Note that $d_{i,k}^{j,\ell} = 0$ for all k, ℓ if $j \notin \partial_i$.

Now, we summarize the process of transmission in every time slot $k \in \{1, 2, \dots, K\}$: (i) Every agent $i \in \mathcal{V}_M$ observes its process $X_{i,k}$ defined in (1) and updates the packet in $Q_{i,i}$. (ii) The i^{th} agent decides whether to transmit a packet or remain silent in the current time slot. (iii) If the i^{th} agent chooses to transmit a packet, it selects a specific packet from $\{Q_{i,l}\}_{l \in \mathcal{V}_M}$ and a specific neighbor $j \in \partial_i$ to transmit it to. (iv) Once all agents determine their actions, transmissions start synchronously. (v) Suppose the receiver of the i^{th} agent is the j^{th} agent, and the transmitted packet is chosen from $Q_{i,\ell}$. If the packet cannot be delivered to the j^{th} agent (e.g., due to a collision), then $d_{i,k}^{j,\ell} = 0$, and collision feedback $c_{i,k}^j = 1$ is given back to the i^{th} agent. Otherwise, if the packet is delivered successfully, then $d_{i,k}^{j,\ell} = 1$. The collision feedback is only available to the senders. (vi) Finally, if $Q_{j,\ell}$ is empty, the j^{th} agent caches the received packet. If $Q_{j,\ell}$ is non-empty but the current packet in $Q_{j,\ell}$ is older (we will define ‘‘old’’ and ‘‘new’’ later) than the received one, the j^{th} agent replaces the current packet with the received one. Otherwise, the transmitted packet (from $Q_{i,\ell}$) will be discarded.

A. Optimization Objectives and Policies

Based on the collection of received samples, each agent can estimate the processes for others. Let $\hat{X}_{i,k}^j$ denote the

¹Since the graph is connected, every agent can receive packets from every other agent.

estimate of $X_{j,k}$ in time slot k from the perspective of the i^{th} agent. By convention, $\hat{X}_{i,k}^i = X_{i,k}^i$ for all i and k , and $\hat{X}_{i,0}^j = 0$ for all $i, j \in \mathcal{V}_M$. We define the average sum of estimation errors (ASEE) as our performance metric:

$$L^\pi(M) = \lim_{K \rightarrow \infty} \mathbb{E}[L_K^\pi] \\ L_K^\pi(M) = \frac{1}{M^2 K} \sum_{k=1}^K \sum_{i=1}^M \sum_{j=1}^M (\hat{X}_{i,k}^j - X_{j,k})^2, \quad (2)$$

where $\pi \in \Pi$ refers to a decentralized sampling and transmission policy in place, and Π is the set of all decentralized sampling and transmission policies. Thus, we need to solve the following optimization problem

$$L(M) := \min_{\pi \in \Pi} L^\pi(M). \quad (3)$$

Let us refine the definition of the policy appearing in (2) and (3) with the following definition.

Definition 1. A *sampling and transmission policy* comprises a sequence of decisions $\{(\mu_{i,k}, \nu_{i,k})\}_{i \in \mathcal{V}_M, k \geq 0}$, with $(\mu_{i,k}, \nu_{i,k})$ denoting the decision pair of the i^{th} agent at time slot k , where

- (i) If $\mu_{i,k} \neq i$, then the i^{th} agent transmits the packet in $Q_{i,\nu_{i,k}}$ to the agent $\mu_{i,k} \in \partial_i$.
- (ii) If $\mu_{i,k} = i$, then the i^{th} agent stays silent, and we artificially set $\nu_{i,k} = i$.

Definition 1 (ii) implies *when to sample*. In Definition 1 (i), $\mu_{i,k}$ represents the decision *who to communicate with*, and $\nu_{i,k}$ specifies the decision *what to transmit*. It is worth noting that policies defined in (1) are different from routing policies. In the former, every agent is able to transmit and cache packets, whereas the latter dictates how routers should make decisions about forwarding data packets.

Our objective is to design *decentralized* sampling and transmission mechanisms to achieve the minimum attainable ASEE $L(M)$ in (3). In time k , every agent chooses its action in a decentralized manner based on its current and past local observations, as well as its past actions. We consider two general classes of policies: oblivious policies and non-oblivious policies. In the former class, decision-making is independent of the processes being monitored, and we will see that the AoI is key in decision-making in this class. In the latter class, decision-making depends on the processes, and AoI is no longer sufficient for decision-making.

B. Age of Information

In this subsection, we establish the age of information in multi-hop networks and relate it to the estimation error.

Let $\tau_{i,j}$ be the generation time of the packet in $Q_{i,j}$. Note that the buffer size of $Q_{i,j}$ is 1, so the current packet is the latest one. The age of information (AoI) [8] with respect to $Q_{i,j}$, denoted by $h_{i,k}^j$, is defined as

$$h_{i,k}^j = k - \tau_{i,j}. \quad (4)$$

Without loss of generality, let $h_{i,0}^j = 0$. Now suppose another packet from the j^{th} agent is delivered to the i^{th} agent. It

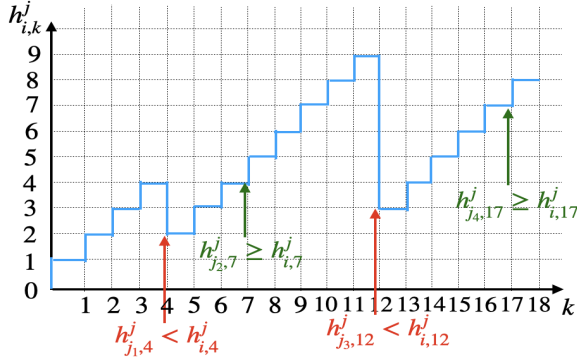


Fig. 1: An example of trajectory of $h_{i,k}^j$.

may be cached in $Q_{i,j}$. Suppose that the delivered packet has generation time τ' and $\tau' < \tau_{i,j}$, i.e., the delivered packet is generated before the current packet in $Q_{i,j}$. If the packet is cached by the i^{th} agent, then the AoI of $Q_{i,j}$ becomes $k - \tau' > k - \tau_{i,j}$, which implies that the delivered packet cannot decrease the AoI of $Q_{i,j}$. In this case, we say that the delivered packet is *older* than the current packet in $Q_{i,j}$, and the i^{th} agent discards the delivered (older) packet and keeps the *newer* one.

Based on (4), the AoI with respect to the j^{th} agent at the i^{th} agent ($h_{i,k}^j$) increases with time, and it jumps down to a certain value when a new packet containing information about the j^{th} agent is received from the u^{th} agent at time slot k ($d_{u,k}^{i,j} = 1$). More precisely, the recursions of $h_{i,k}^j$ are given by

$$h_{i,k+1}^j = \begin{cases} h_{u,k}^j + 1 & d_{u,k}^{i,j} = 1, h_{u,k}^j < h_{i,k}^j \\ h_{i,k}^j + 1 & \text{otherwise.} \end{cases} \quad (5)$$

As an example, in Figure 1, $h_{i,k}^j$ jumps down at time slots 4 and 12, indicating the reception of packets from the j_1^{th} and j_3^{th} agents, respectively. Conversely, $h_{i,k}^j$ increases at time slot 7 and time slot 17, suggesting that the packets received from the j_2^{th} and j_4^{th} agents are stale.

At the beginning of time slot k , the i^{th} agent knows the information of the packet cached in $Q_{i,j}$ before time k , i.e., $X_{j,\tau_{i,j}}$, and reconstructs $\hat{X}_{i,k}^j$ by the Kalman estimator due to its optimality [2]:

$$\hat{X}_{i,k}^j = \mathbb{E}[X_{j,k} | X_{j,\tau_{i,j}}]. \quad (6)$$

In particular, from (1) and (4), we have

$$X_{j,k} = X_{j,\tau_{i,j}} + \sum_{\tau=1}^{h_{i,k}^j} \Lambda_{i,k-\tau}. \quad (7)$$

Since $\mathbb{E}[\Lambda_{i,k}] = 0$ for all i, k , the Kalman estimator in (6) is:

$$\hat{X}_{i,k}^j = \mathbb{E}[X_{j,k} | X_{j,\tau_{i,j}}] = X_{j,\tau_{i,j}}. \quad (8)$$

Based on (8), the recursion of estimates is given by

$$\hat{X}_{i,k+1}^j = \begin{cases} \hat{X}_{u,k}^j & d_{u,k}^{i,j} = 1, h_{u,k}^j < h_{i,k}^j \\ \hat{X}_{i,k}^j & \text{otherwise.} \end{cases} \quad (9)$$

Recalling that our goal to find an optimal decentralized sampling and transmission policy as formulated in (3), we begin by considering oblivious policies. In this setup, the action of node i at time k solely depends on the history of feedback and actions as well as causal observations of the process. Essentially, oblivious policies are independent of the observed processes, making them simpler and less costly to implement. In the following subsection, we show that minimizing ASEE in the class of oblivious policies is equivalent to minimizing the average sum of AoI.

Lemma 1. *In oblivious policies, the expected estimation error associated with process i has the following relationship with the expected age function:*

$$\mathbb{E}[(X_{j,k} - \hat{X}_{i,k}^j)^2] = \mathbb{E}[h_{i,k}^j] \sigma^2. \quad (10)$$

Proof. At the beginning of time slot k , the estimation error is

$$X_{j,k} - \hat{X}_{i,k}^j = X_{j,k} - X_{j,\tau_{i,j}} = \sum_{\tau=1}^{h_{i,k}^j} \Lambda_{i,k-\tau}.$$

It is important to note that under oblivious policies, $h_{i,k}^j$ is independent of $\{\Lambda_{i,k}\}_{i,k}$. Therefore, employing Wald's equality, we obtain

$$\begin{aligned} \mathbb{E}[X_{j,k} - \hat{X}_{i,k}^j] &= 0 \\ \mathbb{E}[(X_{j,k} - \hat{X}_{i,k}^j)^2] &= \mathbb{E}[h_{i,k}^j] \sigma^2. \end{aligned}$$

□

Note that Lemma 1 does not hold for non-oblivious policies. Finding $\mathbb{E}[(X_{j,k} - \hat{X}_{i,k}^j)^2]$ in closed-form is non-trivial and its numerical computation can be intractable when M is large. The challenge arises because even though the estimation error is the sum of $h_{i,k}^j$ Gaussian noise variables, once we condition on $h_{i,k}^j$, their distributions change because $h_{i,k}^j$ can be dependent on the process being monitored. From Lemma 1, in the class of oblivious policies, minimizing the ASEE defined in (11) is equivalent to

$$\min_{\pi \in \Pi'} J^\pi(M), \quad (11)$$

where

$$\begin{aligned} J^\pi(M) &= \lim_{K \rightarrow \infty} \mathbb{E}[J_K^\pi] \\ J_K^\pi(M) &= \frac{1}{M^2 K} \sum_{k=1}^K \sum_{i=1}^M \sum_{j=1}^M h_{i,k}^j, \end{aligned} \quad (12)$$

and Π' is a set of all possible oblivious policies. Later, we will develop a *unified* approach to address both (3) and (11), as outlined in Section IV onwards.

III. PRELIMINARIES

In this section, we introduce the preliminary concepts that will be utilized later. We will leverage the Dec-POMDP framework (see Section III-A) to formulate the problem, employ GNNs and GRNNs (see Section III-B) to construct the graphical actor and critic components, utilize IPPO and MAPPO algorithms (see Section III-D) to train the policy, and demonstrate the transferability of our algorithm using graphons (see Section III-C).

A. Dec-POMDP and Reinforcement Learning

We begin by defining a Decentralized Partially Observable Markov Decision Process (Dec-POMDP) [34]. A Dec-POMDP combines a standard Markov Decision Process to model system dynamics with a hidden Markov model that probabilistically connects the unobservable system states to observations.

Definition 2. A Dec-POMDP can be described by a tuple of key elements $\langle M, S, \{A_i\}_i, P_s, R, \{O_i\}_i, P_o, \gamma \rangle$.

- M : the number of agents.
- S : the set of global environmental states, which are shared by all agents.
- A_i : the action space of the i^{th} agent.
- P_s : $S \times \prod_{i \in \mathcal{V}_M} A_i \times S \rightarrow [0, 1]$ denote the transition probability from a state $s \in S$ to a state $s' \in S$ after executing a (joint) action.
- R : $S \times \prod_{i \in \mathcal{V}_M} A_i \rightarrow \mathbb{R}$ is a global reward function shared by all agents.
- O_i : the observation space of the i^{th} agent.
- P_o : $S \times \prod_{i \in \mathcal{V}_M} O_i \rightarrow [0, 1]$ is the observation function, which provides the probability of a joint observation in a given global environment state.
- $\gamma \in [0, 1]$: the discount factor.

In each time slot k , the environment's state $s_k \in S$ remains unknown to all agents, while each agent i receives its own observations $o_i \in O_i$ without access to other agents' observations. Each agent then selects an action $a_{i,k} \in A_i$ (resulting in a joint action $a_k = (a_{1,k}, \dots, a_{M,k}) \in \prod_{i \in \mathcal{V}_M} A_i$), which prompts the environment to transition to a new state $s'_k \sim P_s(\cdot | s_k, a_k)$. Additionally, the agents collectively receive a global reward $r_k = R(s_k, a_k)$. The entire goal is to devise a policy that maximizes the cumulative discounted reward.

B. Graph Recurrent Neural Networks

We consider a class of RNNs, whose input-output relationship is formulated by equations [50],

$$z_t = \rho_1(Bx_t + Cz_{t-1}), 1 \leq t \leq T, \quad (13)$$

$$\hat{y} = \rho_2(Dz_T). \quad (14)$$

In (13), $\{x_t\}_{1 \leq t \leq T}$ with $x_t \in \mathbb{R}^n$ represents a sequence of n -dimensional data points, $z_t \in \mathbb{R}^n$ is the hidden state extracted from the sequence $\{x_\tau\}_{1 \leq \tau \leq t}$, $B \in \mathbb{R}^{n \times n}$, $C \in \mathbb{R}^{n \times n}$ are linear operators, and ρ_1 is a pointwise nonlinearity. In (14), $\hat{y} \in \mathbb{R}^{n'}$ represents an estimate of $y \in \mathbb{R}^{n'}$, which serves as the target representation of $\{x_t\}_{1 \leq t \leq T}$. Here, $D \in \mathbb{R}^{n \times n'}$ is the linear output map, and ρ_2 is another pointwise nonlinearity. Given a training set $\{\{x_t\}_{1 \leq t \leq T}, y\}$, the optimal linear maps B , C and D are obtained by minimizing some loss function $\mathcal{L}(\rho_2(Dz_T), y)$ over the training set.

We extend x to a graph signal and let Ξ be a graph shift operator (GSO), where $x \in \mathbb{R}^{M \times 1}$, $\Xi \in \mathbb{R}^{M \times M}$, and M is the number of nodes in a graph [15]. Then, we define graph convolutions [15], [51], [52] as follows:

$$B(\Xi)x = \sum_{k=0}^{K-1} b_k \Xi^k x, \quad (15)$$

where $\Xi^k x = \Xi(\Xi^{k-1}x)$ and $b_k \in \mathbb{R}$ for all $0 \leq k \leq K-1$. In (15), K is the order of the graph filter, which is a positive integer hyperparameter, and $\Xi^k x$ represents the information contained in the k -hop neighborhood of each node. For $0 \leq k \leq K-1$, $[b_0, b_1, \dots, b_{K-1}]$ is called filter taps. Combining (13), (14), and (15), the graph recurrent neural network (GRNN) architecture with $\{x_t\}_{1 \leq t \leq T}$ is given by

$$z_t = \rho_1(B(\Xi)x_t + C(\Xi)z_{t-1}), \quad (16)$$

$$\hat{y} = \rho_2(D(\Xi)z_T), \quad (17)$$

where x_t and z_t in (16) and (17) are graph signals.

Suppose each node possesses a vector of features. All feature vectors constitute a graph signal tensor, denoted by $X \in \mathbb{R}^{M \times F}$, where F represents the dimension of feature vectors. Each column $X_f \in \mathbb{R}^M$ is a graph signal corresponding to the values of feature f across all nodes. Extending the linear transformation in (15) to an operator, denoted by $\mathcal{B}(\Xi)$, yields

$$\mathcal{B}(\Xi)V = \sum_{\tau=0}^{K-1} \Xi^\tau X B_\tau, \quad (18)$$

where $B_\tau \in \mathbb{R}^{F \times G}$ with $\tau = 0, 1, 2, \dots, K-1$ represent the filter taps, and G denotes the dimension of the output features.

Finally, suppose the hidden state Z_t has dimension $M \times H$. Considering the graph signal sequences $\{X_t\}_{0 \leq t \leq T}$, (16) and (17) can be extended to

$$Z_t = \rho_1(\mathcal{B}(\Xi)X_t + \mathcal{C}(\Xi)Z_{t-1}), \quad (19)$$

$$\hat{Y} = \rho_2(\mathcal{D}(\Xi)Z_T), \quad (20)$$

where the filter taps are $B_\tau \in \mathbb{R}^{F \times H}$, $C_\tau \in \mathbb{R}^{H \times H}$, and $D_\tau \in \mathbb{R}^{G \times H}$, $\tau = 0, 1, 2, \dots, K-1$. We can represent (19) and (20) more compactly as follows:

$$\hat{Y} = \Phi(\mathcal{B}, \mathcal{C}, \mathcal{D}; \Xi, \{X_t\}_{t=1}^T). \quad (21)$$

C. Graphons

We borrow the description of graphons from [47]. A graphon is the limit of a sequence of dense undirected graphs, defined as $W : [0, 1]^2 \rightarrow [0, 1]$, where W is *bounded*, *measurable* and *symmetric*. The graphon signal is defined as a function $X \in L^2([0, 1])$. An important interpretation of graphons (W) and graphon signals (X) are generative models for graphs and graph signals. A pair (Ξ_n, x_n) can be obtained from the pair (W, X) as follows: a point $u_i \in [0, 1]$ is chosen to be the label of the i^{th} node with $i \in \mathcal{V}_n$. For $1 \leq i, j \leq n$,

$$[\Xi_n]_{ij} = \text{Bernoulli}(W(u_i, u_j)) \quad (22)$$

$$[x_n]_i = X(u_i). \quad (23)$$

For example, *stochastic graphs* can be constructed using the following rule: Let $\{u_i\}_{i=1}^n$ be n points sampled independently and uniformly at random from $[0, 1]$. The n -node stochastic graph \mathcal{G}_n , with GSO Ξ_n , is obtained from W by (22). Conversely, graphons and graphon signals can be induced by graphs and graph signals, respectively. Suppose \mathcal{G}_n is a graph with GSO Ξ_n and node labels $\{u_i\}_{i=1}^n$, where $u_i \in [0, 1]$, and x_n is a graph signal. Define $I_i = [u_i, u_{i+1})$ for $1 \leq i \leq n-1$

and $I_n = [u_n, 1] \cup [0, u_1]$. Then (W_{Ξ_n}, X_n) induced by (Ξ_n, x_n) is given by

$$W_{\Xi_n}(u, v) = \sum_{i=1}^n \sum_{j=1}^n [\Xi_n]_{ij} 1_{u \in I_i} 1_{v \in I_j} \quad (24)$$

$$X_n(u) = \sum_{i=1}^n [x_n]_i 1_{u \in I_i}. \quad (25)$$

The diffusion operator for graphon signals, denoted by T_W , is defined as

$$(T_W X)(v) = \int_0^1 W(u, v) X(u) du. \quad (26)$$

A graphon filter is an operator $T_{B,W}: L^2([0, 1]) \rightarrow L^2([0, 1])$, defined as follows:

$$(T_{B,W} X)(v) = \left(\sum_{k=0}^{K-1} b_k T_W^{(k)} X \right)(v) \quad (27)$$

$$(T_W^{(k)} X)(v) = \int_0^1 W(u, v) (T_W^{(k-1)} X)(u) du,$$

where $T_W^{(0)} = I$ and $[b_0, b_1, \dots, b_{K-1}]$ are the filter coefficients.

A graphon neural network (WNN) is given as follows. At layer ℓ , the incoming $F_{\ell-1}$ features from layer $\ell - 1$ are mapped into F_ℓ features. Denote the features in layer $\ell - 1$ as $X_{\ell-1}^g$, $1 \leq g \leq F_{\ell-1}$ and the features in layer ℓ as X_ℓ^f with $1 \leq f \leq F_\ell$. Then $X_\ell^f = \rho(\sum_{g=1}^{F_{\ell-1}} T_{B_\ell^{fg}, W} X_{\ell-1}^g)$, where $\rho(\cdot)$ is a pointwise nonlinearity and $B_\ell^{fg} = [b_{\ell,0}^{fg}, b_{\ell,1}^{fg}, \dots, b_{\ell,K-1}^{fg}]$. Let $\mathcal{B} \triangleq \{B_\ell^{fg}\}_{\ell,f,g}$ be a tensor grouping the coefficient sets B_ℓ^{fg} for ℓ, f, g . With a slight abuse of notation, we denote $X = \{X_0^g\}_{g=1}^{F_0}$ and $Y = \{X_L^f\}_{f=1}^{F_L}$. A WNN can be represented more compactly as the map

$$Y = T_{\mathcal{B}, W} X. \quad (28)$$

D. A2C Algorithms

We introduce some commonly used reinforcement learning algorithms which will be used in Section VI, namely, IPPO and MAPPO [13], which are variants of the advantage actor-critic (A2C) algorithm [48], [49].

IPPO represents independent learning, where each agent has an actor and a critic trained in a decentralized manner, conditioned on the history of location observations, actions, and rewards, to minimize the loss function. Unlike IPPO, in MAPPO, the critic learns a joint state value function. It extends the existing on-policy actor-critic algorithm A2C [48] by applying centralized critics conditioned on the state of the environment rather than the individual history of observations.

IV. PROPOSED GRAPHICAL REINFORCEMENT LEARNING FRAMEWORK

In this section, we outline the framework of our graphical reinforcement learning algorithm, as depicted in Fig. 2. We start with a general overview and then dive into the details

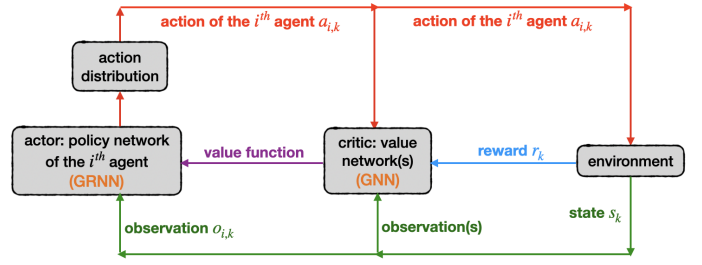


Fig. 2: The proposed graphical reinforcement learning framework.

of two key components: (i) graphical actors and critics and (ii) the action distribution. We will discuss these details in Sections IV-A and IV-B, respectively.

1) *State and Observations*: We begin by detailing the environment state and the observations made by the agents (illustrated by the green arrows in Fig. 2). Denote the adjacency matrix of the network \mathcal{G}_M by Ξ_M . In time slot k , we define the environment state, denoted by s_k , as

$$s_k = \left\{ \{X_{i,k}\}_{i \in \mathcal{V}_M}, \{\hat{X}_{i,k}^j\}_{i,j \in \mathcal{V}_M}, \{h_{i,k}^j\}_{i,j \in \mathcal{V}_M}, \{c_{i,k}^j\}_{i,j \in \mathcal{V}_M}, \{q_{i,k}^j\}_{i,j \in \mathcal{V}_M}, \{d_{i,k}^{j,\ell}\}_{i,j,\ell \in \mathcal{V}_M}, \Xi_M \right\}, \quad (29)$$

which implies that the state s_k includes the physical processes $\{X_{i,k}\}_i$, $\{\hat{X}_{j,k}^i\}_{i,j}$, the age of information $\{h_{j,k}^i\}_{i,j}$, the collision feedback $\{c_{i,k}^j\}_{i,j}$, the indicator of occupation $\{q_{i,k}^j\}_{i,j}$, the indicator of delivery $\{d_{i,k}^{j,\ell}\}_{i,j,\ell}$, and the adjacency matrix Ξ_M . Each node can only observe its local information. Therefore, in time slot k , the observations of the i^{th} agent are denoted as

$$o_{i,k} = \left\{ X_{i,k}, \{\hat{X}_{i,k}^j\}_{j \in \mathcal{V}_M}, \{h_{i,k}^j\}_{j \in \mathcal{V}_M}, \{c_{i,k}^j\}_{j \in \mathcal{V}_M}, \{q_{i,k}^j\}_{j \in \mathcal{V}_M}, \{d_{i,k}^{j,\ell}\}_{j,\ell \in \mathcal{V}_M}, \Xi_M^{(i)} \right\}. \quad (30)$$

Since each agent only knows the adjacent agents, we can explicitly express $[\Xi_M^{(i)}]_{x,y}$ as follows

$$[\Xi_M^{(i)}]_{x,y} = \begin{cases} 1 & \text{if } x = i, y \in \partial_i \text{ or } y = i, x \in \partial_i, \\ 0 & \text{otherwise.} \end{cases}$$

2) *Agents' Actions*: We then outline the actions taken by the agents (the red arrows in Fig. 2). After obtaining the observations, the i^{th} agent makes a decision based on these observations via a policy network (referred to as an actor, to be defined in Section IV-A) and an action distribution (to be defined in Section IV-B). Let the policy network of the i^{th} agent be denoted by $\pi(\cdot | o_{i,k}; \theta_i)$. Since all agents are homogeneous, following prior work in the MARL literature [53], we employ *parameter sharing*, where $\pi(\cdot | o_{i,k}; \theta_i)$ is simplified to $\pi(\cdot | o_{i,k}; \theta)$, where $\theta_1 = \theta_2 = \dots = \theta_M = \theta$. By plugging the output of $\pi(\cdot | o_{i,k}; \theta)$ into the action distribution, we obtain the selected action $a_{i,k} = (\mu_{i,k}, \nu_{i,k})$, where $(\mu_{i,k}, \nu_{i,k})$ is defined in Definition 1 and $a_{i,k}$ is defined in Definition 2. The joint actions $a_k = \{a_{i,k}\}_{i \in \mathcal{V}_M}$ and the state s_k cause the environment transition into the next state $s_{k+1} \sim P_s(\cdot | s_k, a_k)$, where $P_s(\cdot)$ is defined in Definition 2.

²All features are graphon signals.

3) *Rewards*: Next, we delineate the rewards incurred by the selected actions (the blue arrow in Fig. 2). At the end of every time slot k , the environment returns a reward r_k , as defined by

$$r_k = -\frac{\sum_{i,j \in \mathcal{V}_M} (X_{j,k} - \hat{X}_{i,k}^j)^2}{M^2}. \quad (31)$$

The reward is construed as the equal-weighted average estimation error and information from all agents, owing to two primary reasons: (i) agents are statistically identical, and (ii) they cooperatively minimize the ASEE (in (3)). For oblivious policies, as per Lemma 1, the reward simplifies to $r_k = -\frac{\sum_{i,j \in \mathcal{V}_M} h_{i,k}^j}{M^2 K}$. The return $\sum_{\tau=0}^{\infty} \gamma^\tau r_{k+\tau}$ embodies the total accumulated return from time step k , with a discount factor γ .

4) *Updating Process*: Lastly, we explain how the learning model improves itself when receiving rewards (the purple arrow in Fig. 2). To evaluate the effectiveness of different actions, we introduce a value network (referred to as a critic, which will be detailed in Section IV-A). Agents rely on this value network to guide their action choices, favoring those with higher values. Once actions are chosen, they produce a specific reward, which is then fed back into the value network. This prompts the value network to update its parameters based on the received reward. During the training process, we utilize two well-known variants of A2C algorithms: IPPO and MAPPO [48].

A. Graphical Actor and Critic

Now we focus on the construction of the actor and critic. We argue that a graphical structure is necessary. Since agents are located in a wireless network, there exists an inherent network topology among them. Assume that the actor and critic are constructed by deep neural networks. The inputs are a collection of features of nodes in the graph. The outputs of the actor and critic may change if the permutation of nodes changes, even if the environment keeps the same. Therefore, it is crucial for the actor and critic to mitigate the impact of node permutation. To achieve this, we propose utilizing GNNs, as GNNs inherently exhibit permutation invariance [47]. Consequently, we suggest constructing the actor using graph recurrent neural networks (GRNNs), as detailed in Section III-B. GRNNs offer the advantage of fully leveraging the information embedded within the graph structure. Moving forward, we will first outline the actor's construction, followed by a description of the critic.

For the actor, we generate graph signals (as defined in Section III-B) as the inputs, derived from its observations (see (30)). Let us focus on the i^{th} agent and describe the graph signal associated with this agent as follows.

(i) The graph is constructed using the matrix $\Xi_M^{(i)}$ (defined in (30)), denoted by \mathcal{G}_i . It is important to note that \mathcal{G}_i shares the same set of vertices as \mathcal{G} , but with a distinct edge set, determined by the adjacent agents of agent i .

(ii) In this graph, each node j is assigned a node feature, defined as

$$v_{i,k}^j = [(X_{j,k} - X_{i,k}^j)^2, h_{i,k}^j, c_{i,k}^j, [\Xi_M^{(i)}]_{j,i}, e_{i,k}^j]. \quad (32)$$

In (32), $e_{i,k}^j = 1$ indicates that the i^{th} agent sends a new packet to the j^{th} agent during time slot k , while $e_{i,k}^j = 0$ indicates otherwise. Put simply, when $\sum_{\ell} d_{i,k}^{j,\ell} = 1$ and $\sum_{\ell} h_{j,k}^{\ell} < \sum_{\ell} (h_{j,k-1}^{\ell} + 1)$, it follows that $e_{i,k}^j = 1$. For oblivious policies, as per Lemma 1, the node feature $v_{i,k}^j$ can be reduced to $v_{i,k}^j = [h_{i,k}^j, c_{i,k}^j, [\Xi_M^{(i)}]_{j,i}, e_{i,k}^j]$. It is noteworthy that edge features are omitted since the information pertaining to edges is encapsulated within the element $\Xi_M^{(i)}$.

(iii) We denote the dimension of node features as F_0 . In non-oblivious policies, $F_0 = 5$, while in oblivious policies, $F_0 = 4$. We then convert the collection of node features $\{v_{i,k}^j\}_j$ to a graph signal tensor, denoted as $V_{i,0}$, where $V_{i,0} \in \mathbb{R}^{M \times F_0}$.

Upon constructing the graph signals, we introduce L graph recurrent neural network layers. For the ℓ^{th} layer, $1 \leq \ell \leq L$. The input is represented by the output of the $(\ell - 1)^{\text{th}}$ layer, $V_{i,\ell-1} \in \mathbb{R}^{M \times F_{\ell-1}}$, and the output is denoted as $V_{i,\ell} \in \mathbb{R}^{M \times F_{\ell}}$. Similar to (21), we have

$$V_{i,\ell} = \Phi(\mathcal{B}_{\ell}, \mathcal{C}_{\ell}, \mathcal{D}_{\ell}; \Xi_M^{(i)}, \{V_{i,\ell-1}\}_{t=1}^T), \quad (33)$$

where $\mathcal{B}_{\ell}, \mathcal{C}_{\ell}, \mathcal{D}_{\ell}$ are corresponding parameters, T denotes the number of recurrent rounds. In (33), the input $V_{i,\ell-1}$ is utilized repeatedly for T rounds. The parameter θ in the policy network $\pi(\cdot | o_{i,k}; \theta)$ comprises the collection of parameters in the GRNN, i.e., $\theta = \{\mathcal{B}_{\ell}, \mathcal{C}_{\ell}, \mathcal{D}_{\ell}\}_{\ell=1}^L$.

Recalling that we consider two types of RL training, namely, independent learning (IPPO) and centralized training and decentralized execution (MAPPO). The critics in these two training regimes are different since every agent has a distinct critic in the former case, while all agents share a common critic in the latter case.

(i) For the critic in IPPO, the structure is similar to that of the actor. The difference is that we remove the recurrence from the graphical architecture and set $T = 1$.

(ii) For the critic in MAPPO, the state s_k can be known since the critic collects information from all agents. We define the node and edge features as follows. The node feature for the i^{th} agent is defined as $\sum_{j=1}^M [\Xi_M]_{ij}$, i.e., the degree of the i^{th} agent; and the edge feature between i^{th} agent and the j^{th} agent is defined as (32). It is worth noting that we consider ‘‘general edges’’: any pair of agents have an edge to connect each other. If $j \in \partial_i$, then a real edge exists between agent i and agent j ; otherwise the edge is a virtual one. Subsequently, the critic is constructed by substituting node and edge features into (33) and setting $T = 1$.

B. Action Distribution

Consider the i^{th} agent. The output of the actor is computed via (33) and is denoted by $V_{i,L} \in \mathbb{R}^{M \times F_L}$. $V_{i,L}$ is referred to as a node embedding. To select a specific action, we need to feed the node embedding into another operator, which we call an *action distribution*. We denote this operator as ϕ , and it converts a node embedding to an action distribution. In particular, let $\phi: \mathbb{R}^{M \times F_L} \rightarrow \mathbb{R}^{M \times M}$, with the following specific form:

$$\phi(V_{i,L}) := \Delta V_{i,L} \Delta V_{i,L}^T, \quad (34)$$

where $\Delta \in \mathbb{R}^{F_L \times F_L}$ is a learnable parameter matrix. Action $a_{i,k}$ is sampled as follows:

$$a_{i,k} \sim F_{\text{softmax}}(\phi(V_{i,L})). \quad (35)$$

In (34), the number of parameters in ϕ is independent of the number of agents M . Since all agents are homogeneous, they share a common ϕ .

V. FUNDAMENTAL ANALYSIS: TRANSFERABILITY

In this section, we analyze the graphical reinforcement learning framework, starting with the permutation invariance property. It is worth noting that GNNs exhibit the permutation invariance property [54]. Additionally, since a GRNN is a straightforward extension of a GNN combined with an RNN architecture, GRNNs inherit the permutation invariance property [47, Proposition 1].

In practice, learning GNNs for large networks is challenging due to several reasons: (i) acquiring full knowledge of the graph is difficult, especially for large networks, and (ii) matrix multiplication operations become computationally complex as the network size increases. However, the filter taps in a GNN remain independent of the network size. Therefore, models trained on small or moderate graphs can be transferred to large graphs [47].

Suppose y_{n_1} and y_{n_2} are outputs of a GRNN with network sizes n_1 and n_2 , respectively. Transferability implies that the distortion between y_{n_1} and y_{n_2} is small when n_1 and n_2 are large. Since y_{n_1} and y_{n_2} have different dimensions, direct comparison is challenging. Instead, a tractable approach is to compare y_{n_1} or y_{n_2} with their limits. Before delving into transferability, we first introduce some useful notations, definitions and assumptions.

Let W be a graphon, X be a graphon signal, and \mathcal{G}_n be n -node generic graph with node labels $\{u_i\}_{i=1}^n$. Suppose that (Ξ_n, x_n) is induced from (W, X) (see (22) and (23)), and (W_{Ξ_n}, X_n) is induced by (Ξ_n, x_n) (see (24) and (25)). Denote by $T_{B_i, W_{\Xi_n}}$, $i \geq 1$, (generic) graphon filters (see (27)). Denote by $T_{B_i, W_{\Xi_n}}$, $i \geq 1$ a (generic) WNN (see (28)) with L layers, $F_0 = 1$ input feature, $F_L = 1$ output feature, and $F_\ell = F$ features per layer for $1 \leq \ell \leq L-1$. In particular, we call that $B(\Xi_n)$ is a graph filter (see (15)) instantiated from $T_{B,W}$ on the graph Ξ_n , and $\mathcal{B}(\Xi_n)$ is a linear transformation (see (18)) instantiated from $T_{B,W}$ on the graph Ξ_n .

Definition 3. Similar to (19), (20), a graphon recurrent neural network (WRNN) is defined as follows,

$$Z_t = \rho_1(T_{B_1, W} X_t + T_{B_2, W} Z_{t-1}), \quad 1 \leq t \leq T, \quad (36)$$

$$Y = \rho_2(T_{B_3, W} Z_T). \quad (37)$$

To write (36) and (37) compactly,

$$Y = \Psi(B_1, B_2, B_3; W, \{X_t\}_{t=1}^T). \quad (38)$$

Definition 4. ([47, Definition 4]) The ϵ -band cardinality of a graphon W , denoted by κ_W^ϵ , is the number of eigenvalues λ_i of T_W with absolute value larger or equal to ϵ , i.e.,

$$\kappa_W^\epsilon = \#\{\lambda_i : |\lambda_i| \geq \epsilon\}.$$

Definition 5. ([47, Definition 5]) For two graphons W and W' , the ϵ -eigenvalue margin, denoted by $\delta_{WW'}^\epsilon$, is given by

$$\delta_{WW'}^\epsilon = \min_{i,j \neq i} \{|\lambda_i(T_{W'}) - \lambda_j(T_W)| : |\lambda_i(T_{W'})| \geq \epsilon\},$$

where $\lambda_i(T_{W'})$ and $\lambda_i(T_W)$ denote the eigenvalues of $T_{W'}$ and T_W , respectively.

Assumption 1. ([47, Assumption 1]) The spectral response of the convolutional filter of $T_{B,W}$, defined as $b(\lambda) = \sum_{k=0}^{K-1} b_k \lambda^k$, is Ω -Lipschitz in $[-1, -\epsilon] \cup [\epsilon, 1]$ and ω -Lipschitz in $(-\epsilon, \epsilon)$, with $\omega < \Omega$. Moreover, $|b(\lambda)| < 1$.

Under Assumption 1, we can show that if a (large) graph filter is sampled from a graphon, then it can approximate the graphon filter. From Definition 4 and Definition 5, define

$$\Theta(\Omega, \omega) = (\Omega + \frac{\pi \kappa_{W_{\Xi_n}}^\epsilon}{\delta_{WW_{\Xi_n}}^\epsilon}) \|W - W_{\Xi_n}\| + 2\omega\epsilon. \quad (39)$$

Assumption 2. ([47, Assumption 5]) The activation functions are normalized Lipschitz, i.e., $|\rho(x) - \rho(y)| \leq |x - y|$, and $\rho(0) = 0$.

Lemma 2. Let $T_{B_i, W_{\Xi_n}}$, $i \in \{1, 2, \dots, m\}$ satisfy Assumption 1, and $\rho_1, \rho_2, \dots, \rho_{m-1}$ satisfy Assumption 2. Define

$$\begin{cases} Y_n = Z_m, Y = U_m, \\ Z_{i+1} = T_{B_{i+1}, W_{\Xi_n}} Z'_i, Z'_i = \rho_i(Z_i), 1 \leq i \leq m-1 \\ U_{i+1} = T_{B_{i+1}, W} U'_i, U'_i = \rho_i(U_i), 1 \leq i \leq m-1 \\ Z_1 = T_{B_1, W_{\Xi_n}} X_n, U_1 = T_{B_1, W} X \end{cases}$$

For any $0 < \epsilon \leq 1$, it holds that

$$\|Y - Y_n\| \leq \sum_{i=1}^m \Theta(\Omega_i, \omega_i) \|X\| + (\Omega_m \epsilon + 2) \|X - X_n\|,$$

and $\{\Omega_i, \omega_i\}$ are Lipschitz constants associated with $T_{B_i, W_{\Xi_n}}$ for $1 \leq i \leq m$.

Proof. The proof is given in Appendix A. \square

Lemma 3. Let $T_{B_i, W_{\Xi_n}}$, $i \in \{1, 2, \dots, m\}$ satisfy Assumption 1, and $\rho_1, \rho_2, \dots, \rho_{m-1}$ satisfy Assumption 2. Define

$$\begin{cases} Y_n = Z_m, Y = U_m \\ Z_{i+1} = T_{B_{i+1}, W_{\Xi_n}} Z'_i, Z'_i = \rho_i(Z_i), 1 \leq i \leq m-1 \\ U_{i+1} = T_{B_{i+1}, W} U'_i, U'_i = \rho_i(U_i), 1 \leq i \leq m-1 \\ Z_1 = T_{B_1, W_{\Xi_n}} X_n, U_1 = T_{B_1, W} X \end{cases}$$

For any $0 < \epsilon \leq 1$, it holds that

$$\|Y - Y_n\| \leq \sum_{i=1}^m L F^{L-1} \Theta(\Omega_i, \omega_i) \|X\| + (\Omega_m \epsilon + 2) \|X - X_n\|,$$

and $\{\Omega_i, \omega_i\}$ are Lipschitz constants associated with $T_{B_i, W_{\Xi_n}}$ for $1 \leq i \leq m$.

Proof. The proof is given in Appendix B. \square

Theorem 1. (transferability in GRNNs) Let the convolutional filters that makeup of the layers of $T_{B_1, W}$, $T_{B_2, W}$, and $T_{B_3, W}$ satisfy Assumption 1, and ρ_1 and ρ_2 satisfy Assumption 2. Based on (38), define $Y = \Psi(B_1, B_2, B_3; W, \{X_t\}_{t=1}^T)$ and

$Y = \Psi(\mathcal{B}_1, \mathcal{B}_2, \mathcal{B}_3; W, \{X_n\}_{t=1}^T)^3$. For any $0 < \epsilon \leq 1$, it holds that

$$\begin{aligned} \|Y - Y_n\| &\leq LF^{L-1} \sum_{i=1}^3 N_i \Theta(\Omega_i, \omega_i) \|X\| \\ &\quad + (\Omega_3 \epsilon + 2) \|X - X_n\|, \end{aligned} \quad (40)$$

where $\{\Omega_i, \omega_i\}$ are Lipschitz constants associated with $T_{\mathcal{B}_i, W}$ in Assumption 1, and N_1, N_2, N_3 are fixed constants only depends on T .

Proof. From the definition of WRNN in (36) and (37), to prove Theorem 1, we only need to apply Lemma 3 repeatedly. The number of repetitions only depends on T , i.e., the number of recurrences. So, the coefficients N_1, N_2 , and N_3 are fixed and only depend on T . This completes the proof. \square

In the rest of this section, we demonstrate the transferability of action distributions (see (35)). It is important to note that action distributions are discrete. To illustrate transferability, we will compare the action distributions with their continuous action distribution (which will be defined later).

In every learning step, we obtain a matrix Δ (see (34)). Although Δ is updated in the learning process, it remains fixed within each learning step. Define a set of labels

$$f_i = \frac{i-1}{F_L}, \quad 1 \leq i \leq F_L. \quad (41)$$

Let $I_i = [f_i, f_{i+1}]$ for $i = 1, 2, \dots, F_L - 1$ and $I_{F_L} = [f_{F_L}, 1] \cup [0, f_1]$. From (24), we can construct a graphon with respect to Δ as follows,

$$W_\Delta(u, v) = \sum_{i=1}^{F_L} \sum_{j=1}^{F_L} [\Delta]_{ij} \mathbf{1}_{u \in I_i} \mathbf{1}_{v \in I_j}. \quad (42)$$

Substituting (42) into (26) in Section III-C, we obtain the diffusion operator associated with W_Δ , denoted by T_{W_Δ} . Let X_1 and X_2 be any two graphon signals. Substituting $\{X_j\}_{j=1}^2$ into (38), we obtain $\{Y_j\}_{j=1}^2$, respectively, denote

$$\mathcal{X}(Y_1, Y_2) \triangleq \langle Y_1, T_{W_\Delta} Y_2 \rangle, \quad (43)$$

where $\langle \cdot \rangle$ is the inner product.

The continuous version of softmax function F_{softmax} (see (35)), denoted by $\tilde{F}_{\text{softmax}}$, is defined as follows,

$$(\tilde{F}_{\text{softmax}} X)(v) = \frac{e^{X(v)}}{\int_0^1 e^{X(u)} du}. \quad (44)$$

Similar to (44), we define a *continuous action distribution* as

$$A \sim \tilde{F}_{\text{softmax}} \mathcal{X}, \quad (45)$$

and \mathcal{X} is defined in (43).

Let $(\Xi_n, \{x_{n,j}\}_{j=1}^2)$ be induced from $(W, \{X_j\}_{j=1}^2)$, and $(W_{\Xi_n}, \{X_{n,j}\}_{j=1}^2)$ be induced by $(\Xi_n, \{x_{n,j}\}_{j=1}^2)$. Substituting $\{X_{n,j}\}_{j=1}^2$ into (38), we obtain $\{Y_{n,j}\}_{j=1}^2$, respectively. Denote $\mathcal{X}_n(Y_{n,1}, Y_{n,2}) = \langle Y_{n,1}, T_{W_\Delta} Y_{n,2} \rangle$ and $A_n \sim \tilde{F}_{\text{softmax}} \mathcal{X}_n$.

³The inputs X and X_n are utilized repeatedly for T rounds.

Lemma 4. Let the convolutional filters that makeup of the layers of $T_{\mathcal{B}_1, W}$, $T_{\mathcal{B}_2, W}$, and $T_{\mathcal{B}_3, W}$ satisfy Assumption 1, and ρ_1 and ρ_2 satisfy Assumption 2. For any $0 < \epsilon \leq 1$, it holds that

$$\begin{aligned} &\|\mathcal{X}(Y_1, Y_2) - \mathcal{X}_n(Y_{n,1}, Y_{n,2})\| \\ &\leq \|T_{W_\Delta}\| \left(C_N^2 \|X_1\| \cdot \|X_2\| \right. \\ &\quad \left. + C_N (\Omega_3 + 2) (\|X_1\| \|X_2 - X_{n,2}\| + \|X_2\| \|X_1 - X_{n,1}\|) \right. \\ &\quad \left. + (\Omega_3 + 2)^2 \|X_1 - X_{n,1}\| \|X_1 - X_{n,2}\| \right), \end{aligned} \quad (46)$$

where $C_N = LF^{L-1} \sum_{i=1}^3 N_i \Theta(\Omega_i, \omega_i)$, and N_1, N_2, N_3 are given in Theorem 1.

Proof. The proof is given in Appendix C. \square

From the definitions of W_{Ξ_n} , $X_{n,1}$ and $X_{n,2}$, for $\eta > 0$, we can choose large n and small ϵ , such that $\Theta(\Omega_i, \omega_i) < \eta$ for $i \in \{1, 2, 3\}$, $\|X_1 - X_{n,1}\| < \eta$, and $\|X_2 - X_{n,2}\| < \eta$. Lemma 4 implies that $\|\mathcal{X}(Y_1, Y_2) - \mathcal{X}_n(Y_{n,1}, Y_{n,2})\|$ is bounded by a small scalar for any Y_1, Y_2 , and graph \mathcal{G}_n .

Theorem 2. (*transferability in action distributions*) Let the convolutional filters that makeup of the layers of $T_{\mathcal{B}_1, W}$, $T_{\mathcal{B}_2, W}$, and $T_{\mathcal{B}_3, W}$ satisfy Assumption 1, and ρ_1 and ρ_2 satisfy Assumption 2. For any small $\eta > 0$, there exists a $0 < \epsilon \leq 1$ and a large n , such that

$$\|A - A_n\| \leq \Gamma \cdot \eta \quad (47)$$

where Γ is a constant independent of the WRNN defined in (38).

Proof. The proof is given in Appendix D. \square

From Theorem 1 and Theorem 2, we have established the transferability of both GRNNs and action distributions. Therefore, the transferability holds in the proposed framework.

VI. EXPERIMENTAL RESULTS

We confirm our analysis through numerical simulations. The experimental setup and parameters are detailed in Section VI-A, baselines are defined in Section VI-B, and numerical results and discussions are presented in Section VI-C.

A. Experimental Setup

We conduct simulations of the proposed algorithms in both synthetic networks and a real network. For synthetic networks, we utilize Watts–Strogatz graphs with a rewiring probability of 0.5 and $M = 10$ nodes⁴. Other synthetic graphs, such as random geometric graphs, can also be used to model multi-hop wireless networks. For the real network, we select the *aus_simple* network from [55], which consists of 7 connected nodes. In both synthetic and real networks, we set the time horizon of one learning episode to be 1024.

⁴Experiments fail if $M \geq 12$ due to limited computational (GPU) resources.

For the synthetic networks, at the start of each learning episode, we generate a specific type of network graph. Essentially, the models are trained on a sequence of statistically-similar graphs. To assess the performance of the learning-based models during training, we interrupt the training process every 10^{th} episode to evaluate the trained model on a set of 30 test episodes/graphs. As for the real network, all training and testing are conducted on the fixed network in each learning episode. In consideration of space limitations, we have relocated the detailed (hyper)parameters of the experiments to Appendix E.

B. Baselines

To compare our proposed framework, we consider three baselines: (i) classical RL policies, (ii) uniform transmitting policies, and (iii) adaptive age-based policies.

Classical MARL policies: The classical reinforcement learning algorithms used as baselines are described in [13], namely, IPPO and MAPPO. The main distinction between classical reinforcement learning and graphical reinforcement learning (see Section IV) lies in the architecture: in the former case, the actor and critic consist of fully connected neural networks, whereas in the latter case, they comprise graph convolutional layers.

Uniform transmitting policies: In the uniform transmitting policies, each agent decides to transmit to its adjacent agents with equal probability if it caches a packet. The number of packets cached at the side of the i^{th} agent in time slot k is $\sum_{\ell=1}^M q_{i,k}^{\ell}$, and the number of receivers is $\sum_{j=1}^M [\Xi_M]_{ij}$. Then, the total number of actions for the i^{th} agent in time slot k is $1 + (\sum_{j=1}^M q_{i,k}^j) \cdot (\sum_{j=1}^M [\Xi_M]_{ij})$ (the scalar 1 represents the action of being silent). Consequently, the probability of being silent is given by $\frac{1}{1 + (\sum_{\ell=1}^M q_{i,k}^{\ell}) \cdot (\sum_{j=1}^M [\Xi_M]_{ij})}$, and the probability of transmitting the packet in $Q_{i,k}^{\ell}$ to the j^{th} agent is $\frac{1_{\{q_{i,k}^{\ell}=1\}} \cdot 1_{\{[\Xi_M]_{ij}=1\}}}{1 + (\sum_{\ell=1}^M q_{i,k}^{\ell}) \cdot (\sum_{j=1}^M [\Xi_M]_{ij})}$.

Adaptive age-based policies: In the adaptive age-based policies, the goal of the agents is to transmit packets from the cache with small age. Given a fixed scalar $\epsilon > 0$. In time slot k , the i^{th} agent chooses to keep silent with probability $\frac{e^{\epsilon}}{e^{\epsilon} + \sum_{\ell=1}^M 1_{\{q_{i,k}^{\ell}=1\}} \cdot e^{1/(h_{i,k}^{\ell}+1)}}$, and transmits the packet in $Q_{i,\ell}$ to the j^{th} agent with probability $\frac{1}{\sum_{j=1}^M [\Xi_M]_{ij}} \cdot \frac{1_{\{q_{i,k}^{\ell}=1\}} \cdot 1_{\{[\Xi_M]_{ij}=1\}} \cdot e^{1/(h_{i,k}^{\ell}+1)}}{e^{\epsilon} + \sum_{\ell=1}^M 1_{\{q_{i,k}^{\ell}=1\}} \cdot e^{1/(h_{i,k}^{\ell}+1)}}$.

C. Numerical Results

We now proceed to discuss the simulation results. First, we present the performance of our proposed algorithms alongside baseline methods on both synthetic and real networks. Subsequently, we delve into insights regarding transferability. Lastly, we offer a sensitivity analysis of the number of recurrent rounds.

1) *Performance Comparison in Synthetic and Real Networks:*

⁵We use $h_{i,k}^{\ell} + 1$ instead of $h_{i,k}^{\ell}$ to avoid the case when $h_{i,k}^{\ell} = 0$.

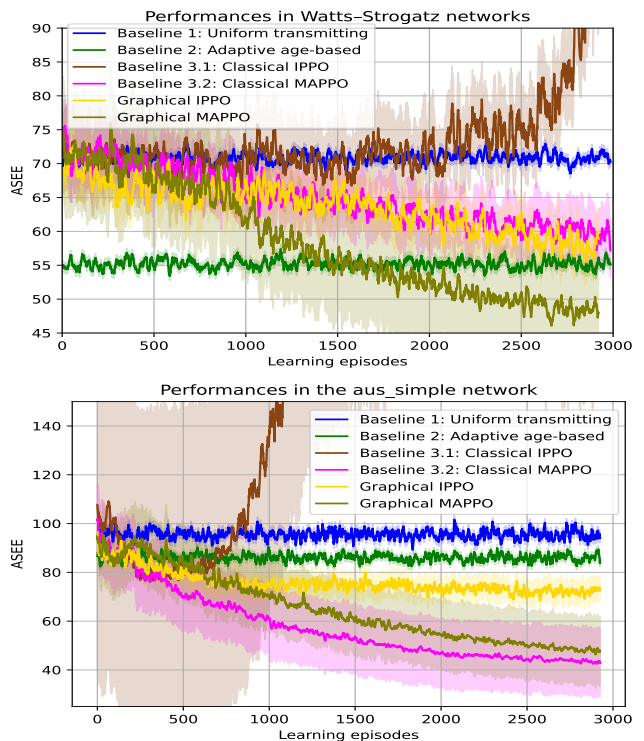


Fig. 3: Performance comparison between the proposed policies and baselines in Watts–Strogatz and the (*aus_simple*) networks.

The ASEE of our proposed policies and baselines in Watts–Strogatz and the real networks are presented in Fig. 3. The ASEE in Watts–Strogatz networks are given in the upper one, from which we derive the following insights: (i) Graphical IPPO policies outperform the classical IPPO policies, and the graphical MAPPO policies outperform the classical MAPPO policies, indicating the superiority of graphical MARL policies over classical MARL policies in our scenario. (ii) Graphical MAPPO policies outperform the adaptive age-based policies, while the adaptive age-based policies outperform graphical IPPO policies. This suggests that CTDE leads to better performance compared to independent learning in our setting. (iii) For classical IPPO policies, the estimation error escalates with learning episodes due to the inherent non-stationarity of independent learning techniques, exacerbated by increasing information. Comparing graphical IPPO policies with classical IPPO policies, we observe that graphical reinforcement learning exhibits greater resilience to non-stationarity.

The ASEE on the real network is detailed in the bottom plot in Fig. 3, showing trends similar to those in the upper one, except for classical and graphical MAPPO policies. Classical MAPPO policies outperform graphical MAPPO policies, which is reasonable in the context of the real network. This difference can be attributed to the fact that the training model in the critic of graphical MAPPO policies is a GNN, while in classical MAPPO policies, it is a neural network, making the former a subset of the latter. Therefore, if the network topology is fixed, the training model in classical MAPPO policies is superior. However, despite their superior performance with a

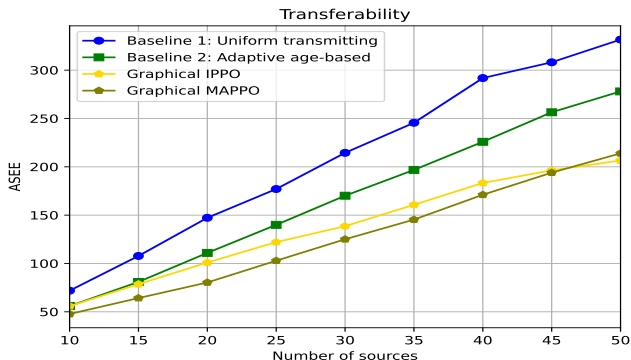


Fig. 4: Transferability of proposed policies in Watts–Strogatz graphs, trained on 10-node networks and tested on networks with $M \in [10, 50]$ nodes.

fixed topology, classical MAPPO policies are less practical than graphical MAPPO policies due to scalability issues and the unbearable learning cost in large-scale networks.

2) *Transferability*: The transferability of our proposed frameworks is illustrated in Figure 4. We apply the models trained on 10-node Watts-Strogatz networks to larger-size networks. The gaps between our proposed policies and baselines increase with the number of sources, indicating that the superiority of our proposed policies in small networks persists in larger networks, and the increased gaps demonstrate the amplified superiority.

Furthermore, the graphical IPPO policies exhibit better transferability than graphical MAPPO policies after reaching a certain network size ($M \approx 45$). This is attributed to the fact that the transferability property holds only within the class of GNN architectures built on graph filters [47]. In contrast, in MAPPO, the critic GNN architectures are not built on graph filters. Therefore, this phenomenon occurs because the critic GNN architecture violates transferability. We believe that selecting critic GNN architectures built on graph filters would lead to graphical MAPPO policies outperforming graphical IPPO policies across all numbers of agents.

3) *Sensitivity Analysis*: We are interested in the ASEEs of proposed policies with ($L = 2$) and without ($L = 1$) recurrence. In Fig. 5, we observe that in both graphical IPPO and graphical MAPPO policies, the ASEEs in policies with recurrence outperform those in policies without recurrence, indicating that recurrence is beneficial in our proposed policies. Furthermore, focusing on the graphical IPPO policies, the ASEEs of those without recurrence initially decrease before increasing, whereas the ASEEs of those with recurrence consistently decrease. Therefore, recurrence can improve resilience to non-stationarity.

VII. CONCLUSION

In this paper, we investigate decentralized sampling and transmission policies to minimize the time-average estimation error and/or time-average age of information in multi-hop wireless networks, considering both oblivious policies and non-oblivious policies. We formulate the age of information and estimation error for all agents within multi-hop networks

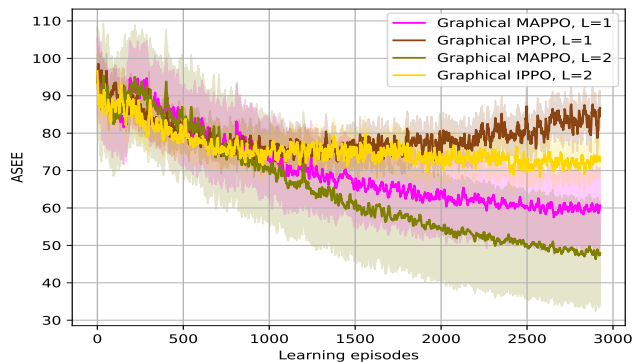


Fig. 5: Performances of proposed policies in the real network under different L .

in a discrete-time setting, and prove that in oblivious policies, minimizing estimation error is equivalent to minimizing the age. Thus, we unify the problems of error and age minimization. To address two key challenges of (i) substantial learning cost associated with scalability, and (ii) the disorder stemming from node permutations in graphs, we propose a scalable graphical reinforcement learning framework. Notably, our proposed framework exhibits the permutation-equivariance property, ensuring consistency in output across different permutations of inputs. Moreover, we prove the transferability of our framework, demonstrating that models trained on small or moderate networks can be applied to large-scale networks directly, thus substantially reducing the learning overhead. Through simulations conducted on both synthetic and real-world networks, we showcase the superiority of our proposed policies over existing state-of-the-art methods, while also validating the transferability of our trained policies.

REFERENCES

- [1] X. Chen, X. Liao and S. Saeedi-Bidokhti, “Real-time sampling and estimation on random access channels: Age of information and beyond,” in *IEEE International Conference on Computer Communications (INFOCOM)*, 2021.
- [2] R. V. Ramakanth, V. Tripathi, and E. Modiano, “Monitoring Correlated Sources: AoI-based Scheduling is Nearly Optimal,” arXiv, 2023.
- [3] Y. Sun, Y. Polyanskiy, and E. Uysal-Biyikoglu, “Sampling of the Wiener process for remote estimation over a channel with random delay,” *IEEE Transactions on Information Theory*, vol. 66, no. 2, pp. 1118 – 1135, 2020.
- [4] T. Z. Ornee and Y. Sun, “Sampling for remote estimation for Ornstein-Uhlenbeck process through queues: age of information and beyond,” *IEEE/ACM Transactions on Networking*, vol. 29, no. 5, pp. 1962 – 1975, 2021.
- [5] S. Kaul, R. D. Yates, and M. Gruteser, “Real-time status: How often should one update?” in *IEEE International Conference on Computer Communications (INFOCOM)*, 2012.
- [6] Y. Sun, Y. Polyanskiy, and E. Uysal-Biyikoglu, “Remote Estimation of the Wiener Process over a Channel with Random Delay,” *IEEE Transactions on Information Theory*, vol. 66, no. 2, pp. 1118 – 1135, 2020.
- [7] R. Talak and E. Modiano, “Age-Delay Tradeoffs in Queueing Systems,” *IEEE Transactions on Information Theory*, vol. 67, no. 3, pp. 1743 – 1758, 2021.
- [8] X. Chen, K. Gatsis, H. Hassani and S. Saeedi-Bidokhti, “Age of information in random access channels,” *IEEE Transactions on Information Theory*, vol. 68, no. 10, pp. 6548 – 6568, 2022.
- [9] O. T. Yavascan and E. Uysal, “Analysis of slotted ALOHA with an age threshold,” *IEEE Journal on Selected Areas in Communications*, vol. 39, no. 5, pp. 1456 – 1470, 2021.

- [10] S. Kang, A. Eryilmaz, and N. B. Shroff, "Remote Tracking of Distributed Dynamic Sources Over a Random Access Channel With One-Bit Updates," *IEEE Transactions on Network Science and Engineering*, vol. 10, no. 4, pp. 1931 – 1941, 2023.
- [11] V. Tripathi, R. Talak, and E. Modiano, "Information freshness in multihop wireless networks," *IEEE Transactions on Information Theory*, vol. 31, no. 2, pp. 784 – 799, 2023.
- [12] N. Jones and E. Modiano, "Minimizing age of information in spatially distributed random access wireless networks," arXiv, Dec 2022.
- [13] G. Papoudakis, F. Christinos, L. Schafer, and etc, "Benchmarking multi-agent deep reinforcement learning algorithms in cooperative tasks," in *Advances in Neural Information Processing Systems*, 2021.
- [14] F. Gama, J. Bruna, and A. Ribeiro, "Stability properties of graph neural networks," *IEEE Transactions on Signal Processing*, vol. 68, pp. 5680 – 5695, 2020.
- [15] L. Ruiz, F. Gama, and A. Ribeiro, "Gated Graph Recurrent Neural Networks," *IEEE Transactions on Signal Processing*, vol. 68, pp. 6303 – 6318, 2020.
- [16] S. Kaul, M. Gruteser, V. Rai, et. al, "Minimizing age of information in vehicular networks," 2011 8th Annual IEEE Communications Society Conference on Sensor, Mesh and Ad Hoc Communications and Networks, 2011.
- [17] I. Kadota and E. Modiano, "Minimizing age of information in wireless networks with stochastic arrivals," *IEEE Transactions on Mobile Computing*, vol. 20, no. 3, pp. 1173 – 1185, 2021.
- [18] R. D. Yates and S. K. Kaul, "The age of information: real-time status updating by multiple sources," *IEEE Transactions on Information Theory*, vol. 65, no. 3, pp. 1807 – 1827, 2019.
- [19] I. Kadota and E. Modiano, "Age of information in random access networks with stochastic arrivals," in *IEEE International Conference on Computer Communications*, 2021.
- [20] S. Farazi, A. G. Klein and D. R. Brown, "Fundamental bounds on the age of information in general multi-hop interference networks," in *IEEE Conference on Computer Communications Workshops*, 2019.
- [21] B. Buyukates, A. Soysal, and S. Ulukus, "Age of information in multihop multicast networks," *Journal of Communications and Networks*, vol. 21, no. 3, pp. 256 – 267, 2019.
- [22] V. Tripathi, R. Talak, and E. Modiano, "Information freshness in multihop wireless networks," *IEEE/ACM Transactions on Networking*, vol. 31, no. 2, pp. 784 – 799, 2022.
- [23] E. Tolstaya, L. Butler, D. Mox, et. al, "Learning connectivity for data distribution in robot teams," in *IEEE/RSJ International Conference on Intelligent Robots and Systems*, 2021.
- [24] Y. Sun, Y. Polyanskiy, and E. Uysal-Biyikoglu, "Remote estimation of the Wiener process over a channel with random delay," in *IEEE International Symposium on Information Theory*, 2017.
- [25] T. Z. Ornee and Y. Sun, "Performance bounds for sampling and remote estimation of Gauss-Markov processes over a noisy channel with random delay," in *IEEE International Workshop on Signal Processing Advances in Wireless Communications*, 2021.
- [26] C. Tsai and C. Wang, "Unifying AoI Minimization and Remote Estimation—Optimal Sensor/Controller Coordination With Random Two-Way Delay," *IEEE/ACM Transactions on Networking*, vol. 30, no. 1, pp. 229 – 242, 2022.
- [27] C. Kam, S. Kompella, G. D. Nguyen, et. al, "Towards an Effective Age of Information: Remote Estimation of a Markov Source," in *IEEE Conference on Computer Communications Workshops*, 2018.
- [28] A. Maatouk, S. Kriouile, M. Assaad, et. al, "The Age of Incorrect Information: A New Performance Metric for Status Updates," *IEEE/ACM Transactions on Networking*, vol. 28, no. 5, pp. 2215 – 2228, 2020.
- [29] S. Saha, H. Makkar, V. Sukumaran, et. al, "On the Relationship Between Mean Absolute Error and Age of Incorrect Information in the Estimation of a Piecewise Linear Signal Over Noisy Channels," *IEEE Communications Letters*, vol. 26, no. 11, pp. 2576 – 2580, 2022.
- [30] P. Hernandez-Leal, B. Kartal and M. E. Taylor, "A survey and critique of multiagent deep reinforcement learning," in *International Conference on Autonomous Agents and Multi-Agent Systems*, 2019.
- [31] M. Tan, "Multi-agent reinforcement learning: Independent vs. cooperative agents," in *International Conference on Machine Learning*, 1993.
- [32] R. Lowe, Y. Wu, A. Tamar, and etc, "Multi-agent actor-critic for mixed cooperative-competitive environments," in *Advances in Neural Information Processing Systems*, 2017.
- [33] P. Sunehag, G. Lever, A. Gruslyns, and etc, "Value-decomposition networks for cooperative multi-agent learning," in *International Conference on Autonomous Agents and Multi-Agent Systems*, 2018.
- [34] A. Feriani and E. Hossain, "Single and Multi-Agent Deep Reinforcement Learning for AI-Enabled Wireless Networks: A Tutorial," *IEEE Communications Survey & Tutorials*, vol. 33, no. 2, pp. 1226 – 1252, 2021.
- [35] N. Naderialzadeh, J. Sydir, M. Simsek, and etc, "Resource Management in Wireless Networks via Multi-Agent Deep Reinforcement Learning," *IEEE Transactions on Wireless Communications*, vol. 20, no. 6, pp. 3507 – 3523, 2021.
- [36] Y. Nasir and D. Guo, "Multi-Agent Deep Reinforcement Learning for Dynamic Power Allocation in Wireless Networks," *IEEE Journal on Selected Areas in Communications*, vol. 37, no. 10, pp. 2239 – 2250, 2019.
- [37] Y. Zhang, B. Di, Z. Zheng, J. Lin, and etc, "Distributed Multi-Cloud Multi-Access Edge Computing by Multi-Agent Reinforcement Learning," *IEEE Transactions on Wireless Communications*, vol. 20, no. 4, pp. 2565 – 2578, 2021.
- [38] H. Li, Y. Wu, and M. Chen, "Adaptive Fault-Tolerant Tracking Control for Discrete-Time Multiagent Systems via Reinforcement Learning Algorithm," *IEEE Transactions on Cybernetics*, vol. 51, no. 3, pp. 1163 – 1174, 2021.
- [39] N. Garg and T. Ratnarajah, "Cooperative Scenarios for Multi-Agent Reinforcement Learning in Wireless Edge Caching," in *IEEE International Conference on Acoustics, Speech and Signal Processing (ICASSP)*, 2021.
- [40] K. Menda, Y. Chen, J. Grana, and etc, "Deep Reinforcement Learning for Event-Driven Multi-Agent Decision Processes," *IEEE Transactions on Intelligent Transportation Systems*, vol. 20, no. 4, pp. 1259 – 1268, 2019.
- [41] M. Gori, G. Mondardini, and F. Scarselli, "A new model for learning in graph domains," in *IEEE International Joint Conference on Neural Networks*, 2005.
- [42] R. Pascanu, C. Gulcehre, K. Cho, and etc, "How to construct deep recurrent neural networks," in *International Conference on Learning Representations*, 2014.
- [43] M. Schuster and K. K. Paliwal, "Bidirectional recurrent neural networks," *IEEE Transactions on Signal Processing*, vol. 45, no. 11, pp. 2673 – 2681, 1997.
- [44] Y. Seo, M. Defferrard, P. Vandergheynst, and etc, "Structured sequence modeling with graph convolutional recurrent networks," in *International Conference on Neural Information Processing*, 2018.
- [45] Y. Li, R. Yu, C. Shahabi, and etc, "Diffusion convolutional recurrent neural network: Data-driven traffic forecasting," in *International Conference on Learning Representations*, 2018.
- [46] C. Capanema, G. Oliveira, F. Silva, and etc, "Combining recurrent and Graph Neural Networks to predict the next place's category," *Ad Hoc Networks*, vol. 138, no. 103016, 2023.
- [47] L. Ruiz, L. F. O. Chamon, and A. Ribeiro, "Transferability Properties of Graph Neural Networks," arXiv, Dec 2021.
- [48] V. Mnih, A. Badia, M. Mirza, and etc, "Asynchronous methods for deep reinforcement learning," in *International Conference on Machine Learning*, 2016.
- [49] P. Dhariwal, C. Hesse, O. Klimov, and etc, "Openai baselines," OpenAI, Tech. Rep., Jan 2020. [Online]. Available: <https://github.com/openai/baselines>
- [50] I. Goodfellow, Y. Bengio, and A. Courville, *Deep Learning (Adaptive Computation and Machine Learning series)*. The MIT Press, 2016.
- [51] F. Gama, A. G. Marques, G. Leus, and A. Ribeiro, "Convolutional Graph Neural Networks," in *The 53rd Asilomar Conference on Circuits, Systems and Computers (ACSSC)*, 2019.
- [52] J. Du, J. Shi, S. Kar, and etc, "On graph convolution for graph CNNs," in *IEEE Data Science Workshop (DSW)*, 2018.
- [53] T. Rashid, M. Samvelyan, C. Schroeder-De-Witt, and etc, "QMIX: monotonic value function factorisation for deep multi-agent reinforcement learning," in *International Conference on Machine Learning*, 2018.
- [54] I. Liu, R. A. Yeh, and A. G. Schwing, "Pic: Permutation invariant critic for multi-agent deep reinforcement learning," arXiv, 2019.
- [55] S. Knight, H. X. Nguyen, N. Falkner, and et.al., "The Internet Topology Zoo," *IEEE Journal on Selected Areas in Communications*, vol. 29, no. 9, pp. 1765 – 1775, 2011.
- [56] [Online]. Available: pytorch-geometric.readthedocs.io/en/latest/
- [57] W. Rudin, *Functional Analysis (Second Edition)*. McGraw-Hill, 1991.
- [58] B. Gao and L. Pavel, "On the Properties of the Softmax Function with Application in Game Theory and Reinforcement Learning," arXiv, Apr 2017.
- [59] A. B. Aleksandrov and V. V. Peller, "Operator Lipschitz functions," *Russian Mathematical Surveys*, vol. 71, no. 4, pp. 605 – 702, 2016.

APPENDIX A
PROOF OF LEMMA 2

It suffices to prove $m = 2$. The proof of the case when $m = 2$ can be extended straightforwardly to the case with any integer m .

First, we utilize the term $T_{B_1, W_{\Xi_n}} \rho_1(T_{B_2, W} X)$ to modify $\|Y_n - Y\|$. By the triangle inequality, we have:

$$\begin{aligned} & \|Y_n - Y\| \\ &= \|T_{B_1}(W_{\Xi_n})\rho_1(T_{B_2, W_{\Xi_n}} X_n) - T_{B_1, W}\rho_1(T_{B_2, W} X)\| \\ &\leq \|T_{B_1, W_{\Xi_n}}\rho_1(T_{B_2, W_{\Xi_n}} X_n) - T_{B_1, W_{\Xi_n}}\rho_1(T_{B_2, W} X)\| \\ &\quad + \|T_{B_1, W_{\Xi_n}}\rho_1(T_{B_2, W} X) - T_{B_1, W}\rho_1(T_{B_2, W} X)\| \\ &\triangleq D_1 + D_2. \end{aligned}$$

We compute D_1 . Note that $T_{B_1, W_{\Xi_n}}$ satisfy Assumption 1, the norm of the operator $T_{B_1, W_{\Xi_n}}$ is bounded by 1, hence

$$\begin{aligned} D_1 &= \|T_{B_1, W_{\Xi_n}}\rho_1(T_{B_2, W_{\Xi_n}} X_n) - T_{B_1, W_{\Xi_n}}\rho_1(T_{B_2, W} X)\| \\ &= \|T_{B_1, W_{\Xi_n}}(\rho_1(T_{B_2, W_{\Xi_n}} X_n) - \rho_1(T_{B_2, W} X))\| \\ &\leq \|\rho_1(T_{B_2, W_{\Xi_n}} X_n) - \rho_1(T_{B_2, W} X)\| \\ &\leq \|T_{B_2, W_{\Xi_n}} X_n - T_{B_2, W} X\| \end{aligned}$$

The last inequality holds due to Assumption 2. From [47, Theorem 1], for any $0 < \epsilon \leq 1$, it holds that

$$\begin{aligned} & \|T_{B_2, W} X - T_{B_2, W_{\Xi_n}} X_n\| \leq \\ & \Theta(\Omega, \omega)\|X\| + (\Omega\epsilon + 2)\|X - X_n\|. \end{aligned} \quad (48)$$

Therefore, by (48),

$$\begin{aligned} & \|T_{B_2, W_{\Xi_n}} X_n - T_{B_2, W} X\| \\ & \leq \Theta(\Omega_2, \omega_2)\|X\| + (\Omega_2\epsilon + 2)\|X - X_n\|. \end{aligned} \quad (49)$$

Note that the activation function ρ_1 is pointwise non-linear. Then, for D_2 , again, by (48), we have:

$$\begin{aligned} D_2 &= \|T_{B_1, W_{\Xi_n}}\rho_1(T_{B_2, W} X) - T_{B_1, W}\rho_1(T_{B_2, W} X)\| \\ & \leq \Theta(\Omega_1, \omega_1)\|\rho_1(T_{B_2, W} X)\|. \end{aligned}$$

Note that $T_{B_2, W}$ satisfies Assumption 1 and ρ satisfies Assumption 2, so $\|\rho_1(T_{B_2, W} X)\| \leq \|T_{B_2, W} X\| \leq \|X\|$. Thus,

$$\begin{aligned} & \|T_{B_1, W_{\Xi_n}}\rho_1(T_{B_2, W} X) - T_{B_1, W}\rho_1(T_{B_2, W} X)\| \\ & \leq \Theta(\Omega_1, \omega_1)\|X\| \end{aligned} \quad (50)$$

From (49) and (50), we obtain the desired results.

APPENDIX B
PROOF OF LEMMA 3

It suffices to prove $m = 2$. The proof of the case when $m = 2$ can be extended straightforwardly to the case with any integer m .

First, we utilize the term $T_{B_1, W_{\Xi_n}} \rho_1(T_{B_2, W} X)$ to modify $\|Y_n - Y\|$. By the triangle inequality, we have

$$\begin{aligned} & \|Y_n - Y\| \\ &= \|T_{B_1, W_{\Xi_n}}\rho_1(T_{B_2, W_{\Xi_n}} X_n) - T_{B_1, W}\rho_1(T_{B_2, W} X)\| \\ &\leq \|T_{B_1, W_{\Xi_n}}\rho_1(T_{B_2, W_{\Xi_n}} X_n) - T_{B_1, W_{\Xi_n}}\rho_1(T_{B_2, W} X)\| \\ &\quad + \|T_{B_1, W_{\Xi_n}}\rho_1(T_{B_2, W} X) - T_{B_1, W}\rho_1(T_{B_2, W} X)\| \\ &\triangleq D_1 + D_2. \end{aligned}$$

For the first term D_1 , note that the convolutional filters that make up its layers all satisfy Assumption 1, hence

$$\begin{aligned} & \|T_{B_1, W_{\Xi_n}}\rho_1(T_{B_2, W_{\Xi_n}} X_n) - T_{B_1, W_{\Xi_n}}\rho_1(T_{B_2, W} X)\| \\ &= \|T_{B_1, W_{\Xi_n}}(\rho_1(T_{B_2, W_{\Xi_n}} X_n) - \rho_1(T_{B_2, W} X))\| \\ &\leq \|\rho_1(T_{B_2, W_{\Xi_n}} X_n) - \rho_1(T_{B_2, W} X)\| \\ &\leq \|T_{B_2, W_{\Xi_n}} X_n - T_{B_2, W} X\|. \end{aligned}$$

The last inequality holds because of Assumption 2. From [15, Theorem 2],

$$\begin{aligned} & \|T_{B_2, W} X - T_{B_2, W_{\Xi_n}} X_n\| \leq \\ & LF^{L-1}\Theta(\Omega, \omega)\|X\| + (\Omega\epsilon + 2)\|X - X_n\|. \end{aligned} \quad (51)$$

Therefore, by (51),

$$\begin{aligned} & \|T_{B_2, W_{\Xi_n}} X_n - T_{B_2, W} X\| \leq LF^{L-1}\Theta(\Omega_2, \omega_2)\|X\| \\ & \quad + (\Omega_2\epsilon + 2)\|X - X_n\|. \end{aligned} \quad (52)$$

For the second term D_2 , again, by (51),

$$\begin{aligned} & \|T_{B_1, W_{\Xi_n}}\rho_1(T_{B_2, W} X) - T_{B_1, W}\rho_1(T_{B_2, W} X)\| \\ & \leq LF^{L-1}\Theta(\Omega_1, \omega_1)\|\rho_1(T_{B_2, W} X)\| \end{aligned}$$

Note that $T_{B_2, W}$ satisfies Assumption 1 and ρ satisfies Assumption 2, so $\|\rho_1(T_{B_2, W} X)\| \leq \|T_{B_2, W} X\| \leq \|X\|$. Thus,

$$\begin{aligned} & \|T_{B_1, W_{\Xi_n}}\rho_1(T_{B_2, W} X) - T_{B_1, W}\rho_1(T_{B_2, W} X)\| \\ & \leq LF^{L-1}\Theta(\Omega_1, \omega_1)\|X\|. \end{aligned} \quad (53)$$

From (52) and (53), we obtain the desired results.

APPENDIX C
PROOF OF LEMMA 4

For any given Δ , from the construction of W_Δ , we know that T_{W_Δ} is continuous. Therefore, T_{W_Δ} is bounded [57], i.e., for any $x \in L^2([0, 1])$, we have $\|T_{W_\Delta} x\| \leq \|T_{W_\Delta}\| \|x\|$. Then, by Cauchy-Schwarz inequality,

$$\begin{aligned} & \|\mathcal{X}(Y_1, Y_2) - \mathcal{X}(Y_{n,1}, Y_{n,2})\| \\ &= \|\langle Y_1 - Y_{n,1}, T_{W_\Delta}(Y_2 - Y_{n,2}) \rangle\| \\ &\leq \|Y_1 - Y_{n,1}\| \cdot \|T_{W_\Delta}(Y_2 - Y_{n,2})\| \\ &\leq \|T_{W_\Delta}\| \|Y_1 - Y_{n,1}\| \|Y_2 - Y_{n,2}\|. \end{aligned}$$

Note that $\|Y_1 - Y_{n,1}\|$ and $\|Y_2 - Y_{n,2}\|$ have been bounded by (40). Substituting (40) into the above equation, we get the desired results.

APPENDIX D
PROOF OF THEOREM 2

Note that $\|A - A_n\| = \|\tilde{F}_{\text{softmax}} \mathcal{X} - \tilde{F}_{\text{softmax}} \mathcal{X}_n\|$. The softmax function F_{softmax} is Lipschit [58], and $\tilde{F}_{\text{softmax}}$ is the continuous version of F_{softmax} . Since $\tilde{F}_{\text{softmax}}$ is in Besov class and is Lipschit [59], there exists a constant Γ , which is independent of the WRNN $\Psi(\mathcal{B}_1, \mathcal{B}_2, \mathcal{B}_3; W, \{X_t\}_{t=1}^T)$, such that

$$\|A - A_n\| = \Gamma \|\mathcal{X} - \mathcal{X}_n\|. \quad (54)$$

The remaining task is to find the upper bound of $\|\mathcal{X} - \mathcal{X}_n\|$.

Since $X_1, X_2 \in L^2([0, 1])$, then $\|X_1\|, \|X_2\| \leq N$, where N is a constant. As $n \rightarrow \infty$, we have $X_{n,1} \rightarrow X_1, X_{n,2} \rightarrow X_2$, and $W_{\Xi_n} \rightarrow W$. For any small $\eta > 0$, we can choose n and ϵ , such that $C_N^2 \|X_1\| \|X_2\| < \frac{\eta}{3\|T_{W_\Delta}\|}$, $(\Omega_3 + 2)^2 \|X_1 - X_{n,1}\| \|X_2 - X_{n,2}\| < \frac{\eta}{3\|T_{W_\Delta}\|}$, and $C_N(\Omega_3 + 2)(\|X_1\| \|X_1 - X_{n,1}\| + \|X_2\| \|X_2 - X_{n,2}\|) < \frac{\eta}{3\|T_{W_\Delta}\|}$, where C_N, Ω_3 are given in Lemma 4. This implies

$$\|\mathcal{X}(Y_1, Y_2) - \mathcal{X}_n(Y_{n,1}, Y_{n,2})\| \leq \eta$$

for any Y_1, Y_2 , and \mathcal{G}_n . Given given Y_1, Y_2 , and $\mathcal{G}_n, Y_{n,1}$ and $Y_{n,2}$ are fixed, so

$$\begin{aligned} & \|\mathcal{X} - \mathcal{X}_n\| \\ & \leq \int_0^1 \int_0^1 \|\mathcal{X}(Y_1, Y_2) - \mathcal{X}_n(Y_{n,1}, Y_{n,2})\| dY_1 dY_2 \\ & \leq \eta, \end{aligned}$$

which gives the desired results.

APPENDIX E

DETAILS OF PARAMETERS IN SECTION VI-C

In the graphical actors and critics, we employ GRNN and GNN architectures, respectively. For our experiments, we configure the networks with 2 layers, each layer having a width of 64. Additionally, we set the number of recurrent rounds to $L = 2$. It is worth noting that there are various GNN modules available [56], and we select suitable GNN modules for the actors and critics in our experiments. These GNN modules serve as hyperparameters in our experiments, and researchers can opt for other GNN modules based on their specific experimental setups. The parameters of the GRNN and GNN architectures are detailed in Table I, while other model and RL framework parameters are summarized in Table II.

Parameters of the GRNN and GNN architectures	Values
Number of layers	2
Width of each layer	64
Number of recurrent rounds	2
GNN module for actors	GCNConv
GNN module for the critic in IPPO	TAGConv
GNN module for the critic in MAPPO	GINEConv

TABLE I: Parameters of the GRNN and GNN architecture.

Other Parameters	Values
The variance of $\Lambda_{i,k}, \sigma^2$	1
The rewiring probability in synthetic networks	0.5
Number of nodes in synthetic networks	10
Number of nodes in the real network	7
Number of testing graphs in synthetic networks	30
Learning rate	0.0003
Learning steps in an episode	1024
Batch size	10
Discount factor	0.99

TABLE II: Model parameters and RL framework parameters.